THE JOURNAL OF PHYSICAL CHEMISTRY C

ARTICLE

pubs.acs.org/JPCC

Size-Dependent Intercalation of Ions into Highly Oriented Pyrolytic Graphite in Ionic Liquids: An Electrochemical Atomic Force Microscopy Study

Pankaj R. Singh and Xiangqun Zeng*

Department of Chemistry, Oakland University, Rochester, Michigan 48309, United States

ABSTRACT: Morphological changes of the highly oriented pyrolytic graphite (HOPG) surface during electrochemical intercalation−deintercalation process in pure ionic liquids (ILs) have been studied using electrochemical atomic force microscopy (EC-AFM). The results show that electrochemical intercalation of ions into HOPG is strongly dependent on anionic size of the ILs used. Up to 0.8 V versus the Ag quasi reference, drastic reversible morphological changes of HOPG surface during anion intercalation−deintercalation were observed in [BMIM][HSO_4], whereas these changes were absent in [BMIM][$N(Tf)_2$]. However, at and above 1.2 V, the HOPG surface degrades in both the ILs to form carbon nanoparticles.

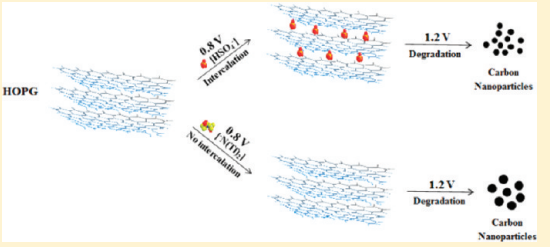

INTRODUCTION

Morphological changes due to electrochemical intercalation−deintercalation of ions during electrochemical processes are a common phenomenon occurring in graphite electrodes. Highly oriented pyrolytic graphite (HOPG) has been widely studied as a model to understand the processes during electrochemical intercalation−deintercalation of ions into graphite. On the basis of Raman spectroscopy, Alsmeyer and McCreery[1] proposed that the intercalation of ions into HOPG in mild aqueous acids is strongly dependent on the identity of the anion. In aqueous 1 M H_2SO_4, 1 M $HClO_4$, and 1 M HNO_3, intercalation was followed by subsequent lattice damage, whereas in 1 M H_3PO_4, neither intercalation nor lattice damage was observed. Blistering was observed on HOPG during intercalation in $NaClO_4/CH_3CN$ as electrolyte, but no lattice damage was observed.[1] Direct evidence for the surface changes of HOPG during intercalation was provided by the pioneering work of Goss and co-workers.[2,3] Using electrochemical atomic force microscopy (EC-AFM), optical microscopy (OM), and scanning electron microscopy (SEM), surface blister formation on HOPG was observed in 1 M KNO_3, 1 M $LiClO_4$, 1 M $(NH_4)_2SO_4$, 1 M HNO_3, and 1 M H_2SO_4 electrolytes. Blister formation on HOPG was also observed in 1 M KOH electrolyte but at significantly higher levels of oxidative charge, whereas blisters were not observed in 1 M K_2HPO_4 and 1 M H_3PO_4 electrolytes. Goss and co-workers proposed blister formation to be due to first intercalation of electrolyte and water into HOPG and then subsequent electrolytic gas evolution at subsurface active sites accompanied by parallel electrolytic formation of graphitic oxide (EGO). EC-AFM studies of the local and time-dependent surface changes of HOPG during intercalation of perchlorate and hydrogen sulfate ions into and their expulsion from HOPG in 2 M $HClO_4$ and 1 M H_2SO_4 have also been done.[4] HOPG expansion with intercalated perchlorate and hydrogen sulfate ions was monitored and was found to depend on the number of HOPG layers involved during intercalation. Blister formation and more dramatic changes in HOPG morphology were observed at higher levels of anion intercalation and also on the kind of electrolyte used.

According to the model proposed by Goss and co-workers,[2,3] solvent (H_2O) molecules play an important role in blister formation during the oxidative reactions on HOPG. Therefore, study of the intercalation−deintercalation process in ionic liquids (ILs) which are composed entirely of ions is of primary significance. However, until now, there are no reports on the AFM study of electrochemical intercalation−deintercalation of ions into HOPG in pure ILs. Being composed entirely of ions, morphological changes in HOPG will be mostly due to intercalation−deintercalation of ions in ILs. ILs have high intrinsic conductivity and show clear advantages over conventional solvents in which use of supporting electrolytes is required for electrochemical study. ILs possesses high ion concentration, high heat capacity, and good electrochemical stability.[5−7] The structure and dynamics at IL/solid interfaces are of fundamental importance in proposed applications of ILs in fields such as catalysis and fuel cells where diffusion of chemical species and electron transfer occur at the interface.[8] IL/solid interfaces have been studied with various techniques including scanning probe microscopy (SPM),[9−14] sum frequency vibrational spectroscopy,[15−17] IR and Raman spectroscopy,[18,19] and neutron reflectrometry.[20] However, there are very few reports on SPM study of IL/HOPG interfaces.[10,21,22] Endres and Freyland[23] used electrochemical scanning tunneling microscopy (EC-STM) to study HOPG in acid room temperature molten salt aluminum chloride-1-methyl-3-butyl-imidazolium chloride. HOPG could be imaged on an atomic scale and at electrode potentials above +1000 mV versus Ag/Ag+ reference; it was oxidized leading to hole etching and protrusions. They proposed intercalation of $AlCl_4^-$ for the protrusions on HOPG. However, dynamics of the etching and

Received: April 25, 2011
Revised: August 2, 2011
Published: August 03, 2011

Scheme 1. Ionic Liquid Intercalation in HOPG

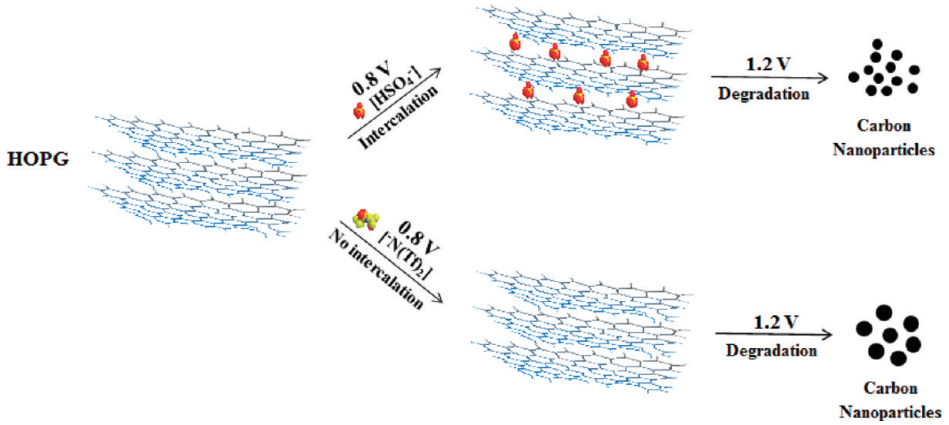

protrusion formation could not be resolved on the time scale of the experiment. Using electrochemistry, Carlin et al.[24] have reported intercalation of organic ion of the buffered neutral ambient-temperature molten salt $AlCl_3$-1-ethyl-3-methylimidazolium chloride and $AlCl_4^-$ into the graphite lattice at the cathodic and anodic limits of the melt, respectively. They found the reversibility of the intercalation−deintercalation of $AlCl_4^-$ to be about 80% and proposed a possible use of conventional graphite rods as electrode material in a dual intercalating molten electrolyte secondary battery.

In the present work, as shown in Scheme 1, we have employed EC-AFM to study morphological changes of HOPG surface during electrochemical intercalation−deintercalation in pure ILs. Two ILs [BMIM][HSO_4] and [BMIM][$N(Tf)_2$] differing in the size and chemical composition of the anion were used for this purpose to see if anionic size has any influence on intercalation into HOPG. [BMIM][HSO_4], a hydrophilic acidic IL, has been used as an efficient and recyclable catalyst for various organic transformations and also acts as a corrosion inhibition agent.[25,26] It has a fairly intercalating [HSO_4^-] anion. On the other hand, [BMIM][$N(Tf)_2$] is a hydrophobic IL and has [$^-N(Tf)_2$] anion which acts as a noncoordinating anion because of delocalization of negative charge along the S−N−S core of the anion.[27] Our results show that electrochemical anion intercalation−deintercalation into HOPG is dependent on the anionic size of the ILs used. Since [BMIM][HSO_4] is a hydrophilic and [BMIM][$N(Tf)_2$] is a hydrophobic IL, there could be effects of hydrophilic/hydrophobic interactions of the ILs with the hydrophobic HOPG surface on the intercalation process. However, these effects may play smaller roles compared to the anionic size effect. Up to 0.8 V versus Ag wire as quasi reference electrode, reversible morphological changes of HOPG surface were observed in [BMIM][HSO_4] because of electrochemical intercalation of [HSO_4^-] into HOPG, whereas no change was observed in [BMIM][$N(Tf)_2$] suggesting absence of intercalation of [$^-N(Tf)_2$] into HOPG. Above 1.2 V, degradation of the HOPG steps to form carbon nanoparticles was observed in both the ILs.

EXPERIMENTAL SECTION

HOPG (12 × 12 × 2 mm) of ZYH grade (Advanced Ceramics Corporation, Lakewood, OH, United States) was used as working electrode. 1-Butyl-3-methyl imidazolium hydrogen sulfate ([BMIM][HSO_4]) with 99% purity was obtained from Iolitec Technologies, Germany. 1-Butyl-3-methyl imidazolium bis(trifluoromethylsulfonyl)imide ([BMIM][$N(Tf)_2$]) was synthesized by Dr. Gary Baker (University of Missouri-Columbia, MO) with purity over 98%.[28−30] These ILs are stable at room temperature and were used without further purification.

All the AFM images were acquired at room temperature in AC mode at a scan rate of 1.0 lines/s with a PicoPlus atomic force microscope from Agilent Technologies, CA, United States. Au coated etched silicon probes of resonant frequency 75 kHz and of spring constant 3.5 N/m were used for all the EC-AFM experiments in pure ILs. Each AFM image was acquired at 512 × 512 resolution. HOPG surface was freshly cleaved with adhesive tape before each experiment. Aluminum foil was used to make electrical contact of the HOPG with the working electrode contact point on the AFM sample plate. One hundred microliters of IL was used as an electrolyte on the freshly cleaved HOPG surface for the EC-AFM experiments. Care was taken to avoid overflow of the added IL. Other parts of the sample plate were electrically insulated by covering them with insulation tape. Ag and Pt wires as quasi reference and counter electrodes, respectively, were then immersed into the IL, and the other side of the wires were connected to the respective contact points on the AFM sample plate. Potentials at the HOPG working electrode were controlled with the help of an in-built potentiostat supplied with the AFM instrument.

The height of the HOPG step was calculated according to the reported procedure[4] and was obtained by calculating the difference between the mean values of height measured in two marked areas on the top and bottom layers of the step thus averaging out the noise contributions and the statistical fluctuations in the measured height. The particle size analysis was done by manually selecting the individual particles in the AFM image and by measuring its size using the AFM software provided with the instrument. A sufficiently large number of particles in a uniform area in the AFM image was selected for this purpose. The frequency of occurrence of a particle of particular size was plotted against particle size to get a histogram. This procedure eliminates any noise contributions to the measured particle size.

RESULTS AND DISCUSSION

Figure 1 shows the molecular structures and physical properties of the ILs used in this study. Since [BMIM][HSO_4] is 80 times more viscous than [BMIM][$N(Tf)_2$], it was fairly difficult to perform EC-AFM experiments in [BMIM][HSO_4] as compared

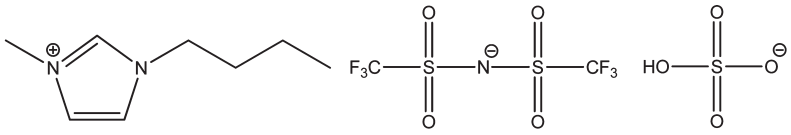

ILs	Viscosity/mPa s	Density/gcm^{-3}	Molecular Volume/nm^3	Ion Pair Diameter/nm
[BMIM][N(Tf)$_2$]	52	1.43	0.49	0.79
[BMIM][HSO$_4$]	4320	1.27	0.31	0.67

Figure 1. Molecular structures and physical properties of the ionic liquids (ILs) used in this study.

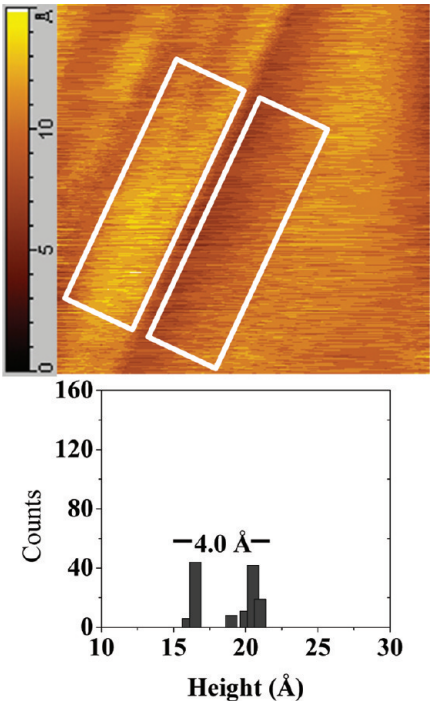

Figure 2. AFM image of HOPG in pure [BMIM][HSO$_4$] at open-circuit potential (OCP). Scan area and height scale for the image are 1 × 1 μm^2 and 15 Å, respectively.

to [BMIM][N(Tf)$_2$]. Molecular volume and ion-pair diameter of [BMIM][N(Tf)$_2$] has been mentioned in the literature.[22] A similar method was adopted to calculate molecular volume and ion-pair diameter of [BMIM][HSO$_4$].

EC-AFM Study of HOPG in Pure [BMIM][HSO$_4$] Up to 0.8 V. Figure 2 shows the AFM image of the HOPG surface in pure [BMIM][HSO$_4$] at open-circuit potential (OCP). An HOPG step of 4 Å, estimated from the difference in the mean values of the heights of terraces in the marked areas, is shown in the image. This particular step was monitored with change in the electrochemical potential at HOPG. Figure 3 shows sequentially obtained EC-AFM images of HOPG in [BMIM][HSO$_4$] at various potentials and intercalation time of 4 min at each potential. At 0.2 V, there was a slight increase in the step height to 4.89 Å (Figure 3a). Considering the smaller molecular volume (Figure 1) of [BMIM]-[HSO$_4$] and good intercalating property of [HSO$_4^-$] anion, the increase in the step height of HOPG is possibly due to intercalation of [HSO$_4^-$] ions into the HOPG layers. According to earlier reports, there are several possible phenomena which can lead to charge-induced dimensional changes in graphite: (1) an increase of interlayer distance upon ion intercalation between adjacent basal planes, (2) widening of the intralayer C−C bond length upon electron injection into the aromatic planes (and shrinking upon hole injection), and (3) an expansion due to the decrease of surface tension with increasing excess charge in the electrochemical double layer.[31,32] The amount of expansion due to widening of intralayer C−C bond length and decrease of surface tension with increasing excess charge in the electrochemical double layer is not more than 1.5% and 0.05%, respectively. Therefore, the thickness change amounting to 22% at 0.2 V compared to that at OCP of the HOPG step during the positive polarization is caused by [HSO$_4^-$] intercalation into HOPG layers. As the potential was further increased to 0.5 V, the step height increased to 5.88 Å as seen in Figure 3b. The thickness change of the step was 20% compared to that at 0.2 V and 47% compared to that at OCP. This clearly shows intercalation of increasing number of [HSO$_4^-$] ions into HOPG with change in the electrode potential to more positive values. To see the reversibility of the intercalation process, the potential was switched back to 0.2 V. Interestingly, the height of the step decreased to 5.19 Å (Figure 3c) suggesting deintercalation of the [HSO$_4^-$] ions from the HOPG. This shows that the intercalation−deintercalation process is reversible. Further increase in the potential to 0.8 V resulted in even greater change in step height to 7.9 Å suggesting a larger volume of intercalated [HSO$_4^-$] ions within the HOPG layers as seen in the AFM image in Figure 3d. The thickness change in this case was 61% relative to that at 0.2 V. According to the literature, interlayer spacing in graphite is 3.35 Å and interlayer spacing upon incorporation of [HSO$_4^-$] ions is 7.98 Å.[33] Hence, the theoretical value for the thickness change is about 138%. However, these results are for intercalation into graphite from H_2SO_4 as electrolyte. The thickness change of the step during intercalation in [BMIM][HSO$_4$] at 0.8 V (Figure 3d) compared to that at OCP (Figure 2) is 97%, which is closer to the theoretical value. To confirm the reversibility of intercalation−deintercalation of [HSO$_4^-$] ions into HOPG, the potential was again switched back to 0.2 V. The AFM image in Figure 3e shows that the intercalated [HSO$_4^-$] ions deintercalates at 0.2 V leading to the decrease in the step height to 5.51 Å. The morphology of the step in Figure 3e looks similar to that in Figure 3c. However, there was a slight degradation of the step (at the upper corner in Figure 3e) because of the continuous intercalation−deintercalation process. The HOPG step height again increased to 7.4 Å as

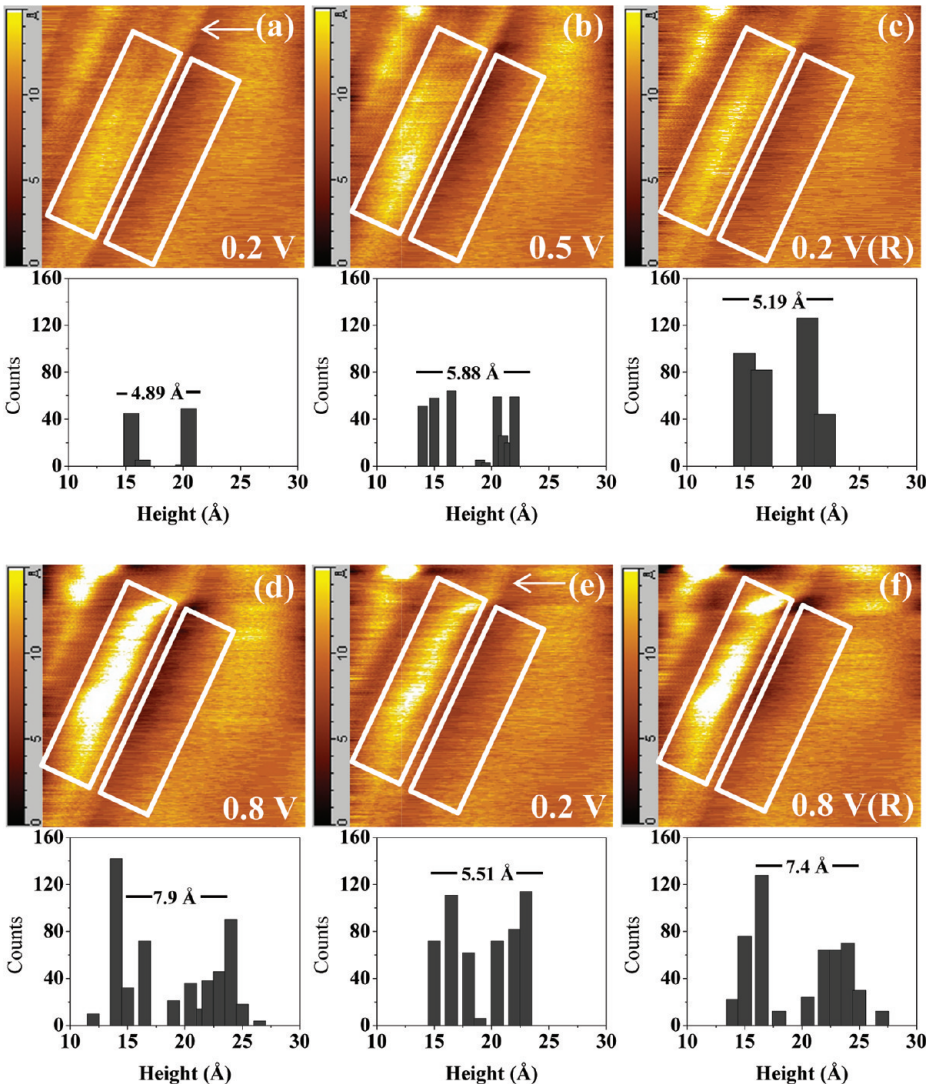

Figure 3. Sequentially obtained EC-AFM images of HOPG in pure [BMIM][HSO_4] at (a) 0.2 V, (b) 0.5 V, (c) 0.2 V (return), (d) 0.8 V, (e) 0.2 V, and (f) 0.8 V (return). All the potentials are vs Ag wire as quasi reference electrode. Scan area and height scale for all the images are 1 × 1 μm^2 and 15 Å, respectively. Acquisition time for each AFM image is 4 min.

the potential was returned back to 0.8 V (Figure 3f). These results demonstrate the reversibility of the morphological changes during the electrochemical intercalation−deintercalation process. These results are based on the assumption that only [HSO_4^-] ions from [BMIM][HSO_4] intercalate into HOPG layers at these potentials. The main reaction leading to the morphological changes in HOPG is

$$[C_x] + [A^-] = [C_x{}^+A^-] + e^- \quad (1)$$

where [C_x] is carbon atoms in HOPG and [A^-] is [HSO_4^-]. Since ILs are composed entirely of ions, we have excluded the contribution of solvent in the above equation. As shown by EC-AFM images, the above reaction is reversible up to 0.8 V. The reversibility of intercalation−deintercalation of [HSO_4^-] ions into HOPG layers is also supported by the cyclic voltammetry (CV) results discussed later (Figure 12a) where only a slight increase in the anodic current was observed up to 0.8 V.

EC-AFM Study of HOPG in Pure [BMIM][HSO_4] above 0.8 V. To observe the effect of more positive potentials (>0.8 V) on the intercalation−deintercalation of [HSO_4^-] ions into HOPG, EC-AFM images of the HOPG step at the same location as discussed in the previous section were monitored on application of more positive potentials. Figure 4a shows the AFM image of the HOPG step at 1.2 V. Drastic degradation of the original step leading to a very thin step was observed at this potential. This suggests that at 1.2 V, because of a large volume of [HSO_4^-] ion intercalation and subsequent HOPG surface oxidation, there is degradation of the step. This is also supported by the observation of large anodic current at 1.2 V in Figure 12a. Further increase in the potentials to 1.5 and 2.0 V in Figure 4b and c, respectively, accelerates the step degradation, and it is barely seen in the AFM image at 2.0 V. Switching back the potential to 0.2 V in Figure 4d hardly changes the morphology of the step suggesting that the degradation process is irreversible. To see the degradation products, after the three potential hold cycles, the HOPG surface with the IL was left overnight for the degradation products to settle. After removal of the IL from the HOPG surface the previous day, the surface was washed with ethanol before AFM imaging. Figure 5 shows the AFM image of the HOPG surface. The

dx.doi.org/10.1021/jp203833v |J. Phys. Chem. C 2011, 115, 17429–17439

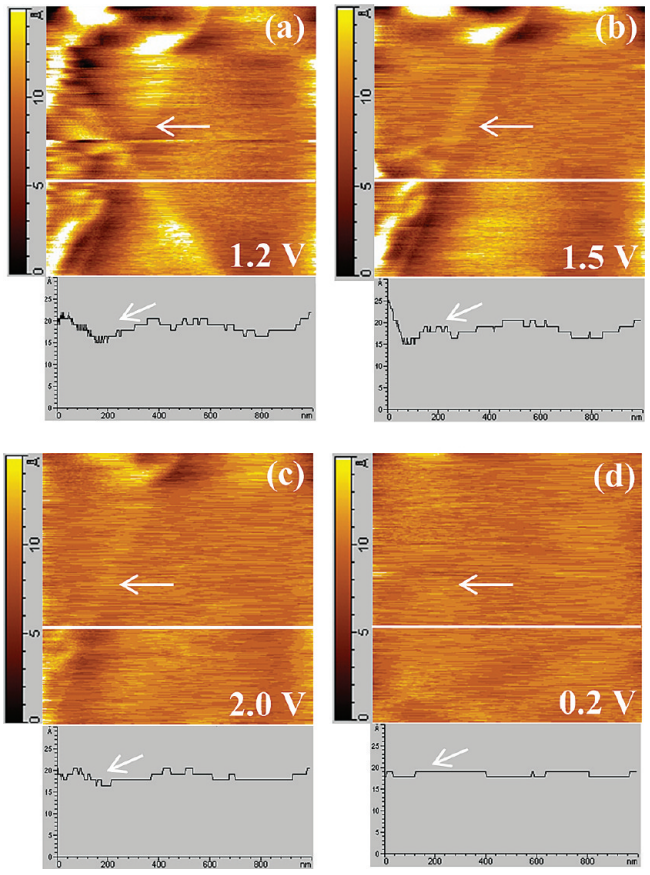

Figure 4. Sequentially obtained EC-AFM images of HOPG in pure [BMIM][HSO_4] at (a) 1.2 V, (b) 1.5 V, (c) 2.0 V, and (d) 0.2 V. All the potentials are vs Ag quasi reference electrode. Scan area and height scale for all the images are 1 × 1 μm^2 and 15 Å, respectively. Acquisition time for each AFM image is 4 min.

15−30 nm size carbon nanoparticles (as shown by the size distribution profile in the inset in Figure 5) are seen adsorbed on the HOPG surface. These particles are the degradation products of the HOPG steps. These results suggest that at and above 1.2 V, most of the steps on the HOPG surface degrade leading to the formation of carbon nanoparticles. Similar observations of degradation of HOPG basal planes to form fine cracks and blisters were observed during the electrochemical intercalation process of lithium into HOPG in 1 M $LiClO_4$ in ethylene carbonate:propylene carbonate (1:2) electrolyte by AFM.[34]

EC-AFM Study of HOPG in Pure [BMIM][$N(Tf)_2$] Up to 0.8 V. To investigate the effect of the size of the anion on the intercalation−deintercalation process into HOPG, EC-AFM images of the HOPG surface in pure [BMIM][$N(Tf)_2$] having the same cation but larger anion were monitored with change in the electrochemical potential. Figure 6 shows the AFM image of the HOPG surface in pure [BMIM][$N(Tf)_2$] at OCP. A HOPG step of 2.75 Å in height can be seen in the image. This particular step was monitored at controlled electrochemical potentials at HOPG to elucidate the effect of intercalation−deintercalation into HOPG layers. Figure 7 shows sequentially obtained EC-AFM images of the HOPG step in [BMIM][$N(Tf)_2$] at various potentials and at intercalation time of 4 min at each potential. Figure 7a is the AFM image at 0.2 V. No change in the step height was observed at this potential when compared with that at OCP.

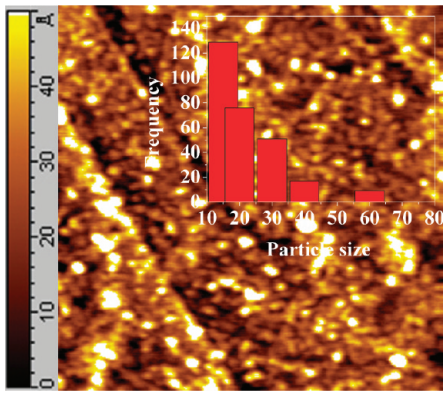

Figure 5. AFM image of the carbon nanoparticles on the HOPG surface. The AFM image was recorded after three potential hold cycles in pure [BMIM][HSO_4] and by allowing the carbon nanoparticles to settle on the HOPG surface for overnight. The HOPG surface was washed with ethanol before AFM imaging. Scan area and height scale for the image are 1 × 1 μm^2 and 50 Å, respectively.

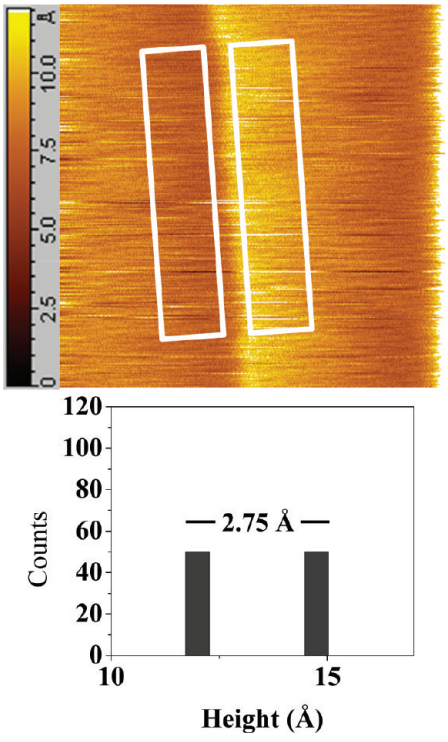

Figure 6. AFM image of HOPG in pure [BMIM][$N(Tf)_2$] at open-circuit potential (OCP). Scan area and height scale for the image are 1 × 1 μm^2 and 12 Å, respectively.

This shows very little or no intercalation of the [$^-N(Tf)_2$] anion into HOPG layers. Figure 7b shows the AFM image of the step at 0.5 V. Here again, no change in the step height of the HOPG was observed suggesting no intercalation. These results are in contrast with that observed for [BMIM][HSO_4] IL discussed earlier. As mentioned in Figure 1, the molecular volume of [BMIM]-[$N(Tf)_2$] is fairly large as compared to [BMIM][HSO_4], and also [$^-N(Tf)_2$] anion is bulky and noncoordinating. Therefore, it is difficult for [$^-N(Tf)_2$] ions to intercalate into the layers of HOPG. Similar to the case of [HSO_4^-] ions, the potential was switched back

dx.doi.org/10.1021/jp203833v |J. Phys. Chem. C 2011, 115, 17429–17439

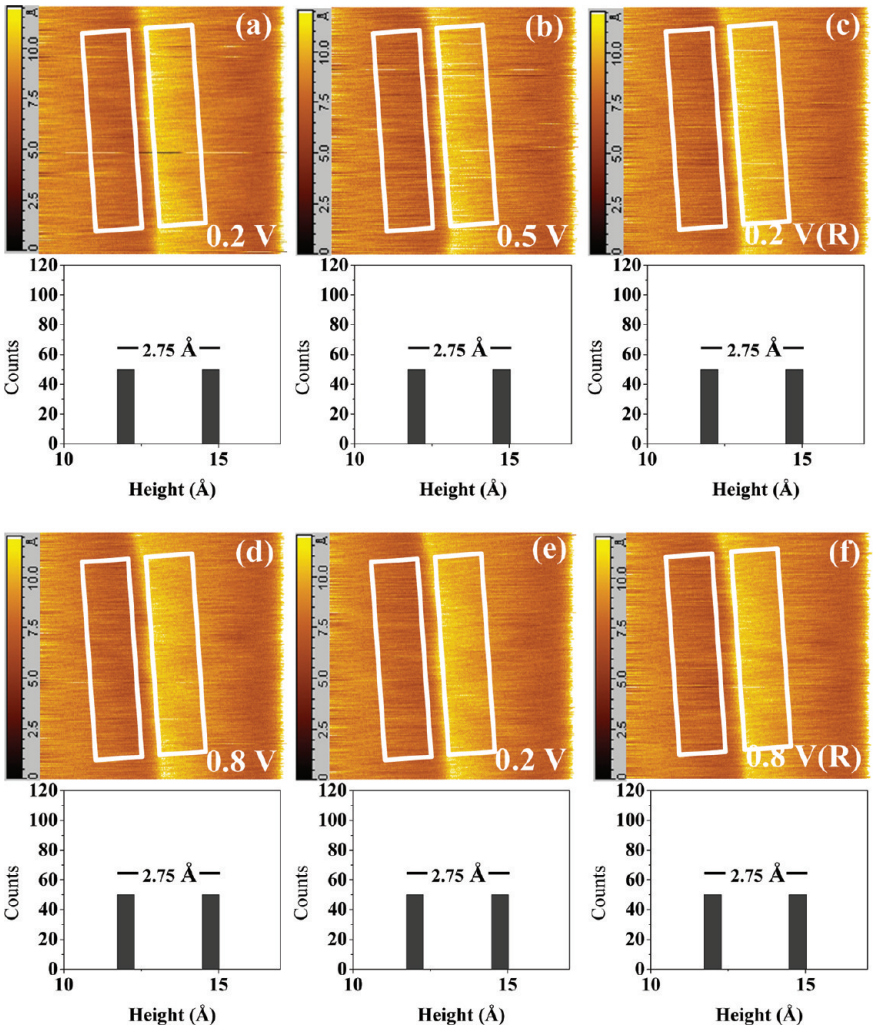

Figure 7. Sequentially obtained EC-AFM images of HOPG in pure $[BMIM][N(Tf)_2]$ at (a) 0.2 V, (b) 0.5 V, (c) 0.2 V (return), (d) 0.8 V, (e) 0.2 V, and (f) 0.8 V (return). All the potentials are vs Ag quasi reference electrode. Scan area and height scale for all the images are $1 \times 1\ \mu m^2$ and 12 Å, respectively. Acquisition time for each AFM image is 4 min.

to 0.2 V to see the reversibility. Figure 7c shows the AFM image recorded at this potential. The image shows no change in the step height (2.75 Å). This further confirms the absence of intercalation of $[^-N(Tf)_2]$ anion into the HOPG layers. Since it was observed before in the case of $[HSO_4^-]$ ion that increasing the potential to more positive values leads to greater intercalation of $[HSO_4^-]$ ions into HOPG layers, EC-AFM images of the HOPG step were also monitored in the presence of $[^-N(Tf)_2]$ anion to ascertain the effect of more positive potential on intercalation of $[^-N(Tf)_2]$ ions into HOPG layers. Figure 7d shows the AFM image of the step at 0.8 V. Here also, no change in the step height (2.75 Å) was observed and hence no intercalation of $[^-N(Tf)_2]$ ions into HOPG. To repeat the process as in the case of $[HSO_4^-]$ ions, the potential was switched back to 0.2 V and the AFM image was recorded. As can be seen in Figure 7e, there was hardly any change in the step height. A similar result was observed when the potential was switched to 0.8 V in Figure 7f. These results suggest that there is no intercalation−deintercalation of $[^-N(Tf)_2]$ ions into HOPG layers in pure $[BMIM][N(Tf)_2]$ up to potential of 0.8 V. CV of HOPG in $[BMIM][N(Tf)_2]$ in Figure 12b also supports this observation where a slight increase in the anodic current was observed up to 0.8 V with no subsequent $[^-N(Tf)_2]$ ion intercalation into HOPG layers (as shown by EC-AFM images). The fact that there was no change in the HOPG step height observed during the EC-AFM studies in $[BMIM][N(Tf)_2]$ confirms our earlier observation that the HOPG step height changes with change in the electrochemical potential in $[BMIM][HSO_4]$ are due to intercalation−deintercalation of $[HSO_4^-]$ ions into HOPG layers and are not due to some electrostatic interactions between the AFM tip and the HOPG surface or to any other such effects.

EC-AFM Study of HOPG in Pure $[BMIM][N(Tf)_2]$ above 0.8 V. When the potential at HOPG in pure $[BMIM][N(Tf)_2]$ was increased to 1.2 V, a drastic change in the surface morphology of HOPG was observed possibly because of HOPG surface oxidation and subsequent intercalation of $[^-N(Tf)_2]$ ions into HOPG layers. This is clearly evident in the AFM image in Figure 8a. A large anodic current at 1.2 V as seen in Figure 12b for the CV of HOPG in $[BMIM][N(Tf)_2]$ also supports this observation. The interface (marked by an arrow) of the initial HOPG step and the step after surface oxidation can be easily observed in Figure 8a. The variation in the surface height is more than 10 Å as seen from the cross section suggesting that there is surface oxidation of HOPG with simultaneous $[^-N(Tf)_2]$ ion intercalation into

dx.doi.org/10.1021/jp203833v |J. Phys. Chem. C 2011, 115, 17429–17439

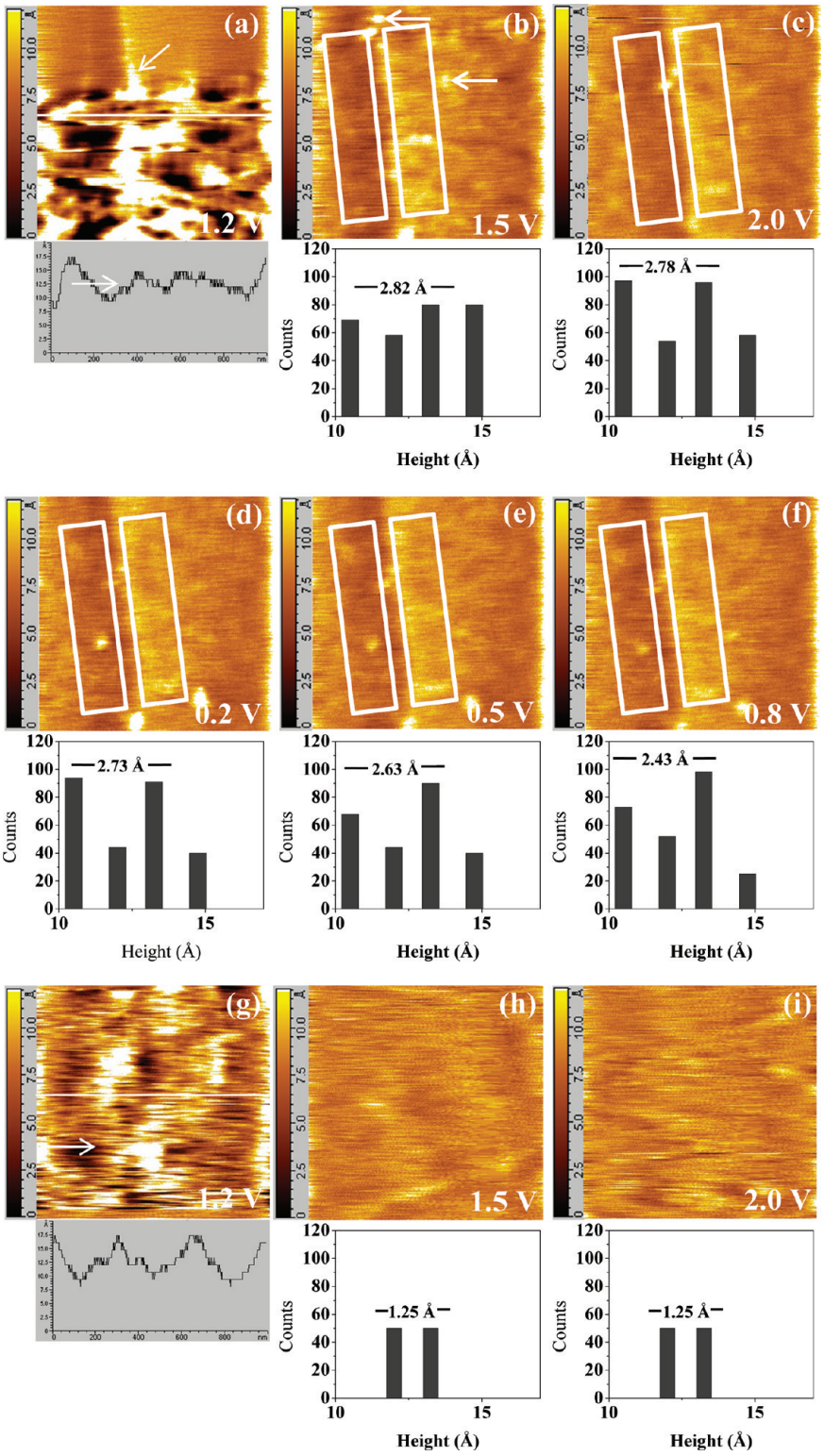

Figure 8. Sequentially obtained EC-AFM images of HOPG in pure [BMIM][N(Tf)$_2$] for the first cycle at (a) 1.2 V, (b) 1.5 V, (c) 2.0 V, (d) 0.2 V, (e) 0.5 V, and (f) 0.8 V and for the second cycle at (g) 1.2 V, (h) 1.5 V, and (i) 2.0 V. All the potentials are vs Ag quasi reference electrode. Scan area and height scale for all the images are 1 × 1 μm^2 and 12 Å, respectively. Acquisition time for each AFM image is 4 min.

HOPG. Figure 8b shows the AFM image of the HOPG surface at the same location at 1.5 V. On comparing the AFM image with that in Figure 7f, it is evident that the carbon layer is removed from the surface. The fact that there is variation in the height distribution profile of the two terraces of the HOPG surface and a slight increase in the HOPG step height to 2.82 Å suggests that there is surface oxidation and simultaneous [$^-$N(Tf)$_2$] ion intercalation into HOPG layers. The AFM image in Figure 8b

dx.doi.org/10.1021/jp203833v |J. Phys. Chem. C 2011, 115, 17429–17439

also shows the presence of particles of 20−25 nm in diameter (shown by arrows in the image) on the HOPG surface. These are possibly particles formed after the graphite oxidation process. There was a slight decrease in the HOPG step height to 2.78 Å when the potential was changed to 2.0 V as seen in Figure 8c. To see if we can sequentially remove more carbon layers from the HOPG surface, the process was repeated. As can be seen from the AFM images in Figure 8d−f, there was hardly any change in the morphology of the HOPG surface at potentials 0.2, 0.5, and 0.8 V, respectively. However, a continuous decrease in the HOPG step height was observed from 2.73 Å (at 0.2 V) to 2.63 Å (at 0.5 V) and 2.43 Å (at 0.8 V). This again suggests carbon layer removal from the HOPG surface. On further increasing the potential to 1.2 V (Figure 8g), a drastic change in the surface morphology of the HOPG surface was observed because of surface oxidation and subsequent intercalation of $[^{-}N(Tf)_2]$ ions into HOPG layers. This is clearly observed in the cross section along the image. After the second oxidation step, it can be seen that the HOPG step, which was clearly visible before oxidation, completely disappears from the HOPG surface at 1.5 V as evident from the AFM image in Figure 8h. The height distribution profile shows a 1.25 Å difference in the HOPG surface height suggesting the flattening of the surface because of removal of the HOPG step. On further increasing the potential to more positive values (at 2.0 V in Figure 8i), there was hardly any change in the surface morphology and height distribution profile of the HOPG surface. These results are similar to our observations of HOPG step oxidation in $[BMIM][HSO_4]$ above 1.2 V. However, as shown by the EC-AFM results, in the case of $[BMIM][N(Tf)_2]$, it is possible to remove carbon layers sequentially by oxidative potential cycling. This suggests that the oxidation process is slower in this case, whereas in the case of $[BMIM][HSO_4]$, multiple carbon layers were removed during the oxidative potential cycling. This is also supported by the CVs of HOPG in both the ILs as shown later in Figure 12a and b where decrease in the anodic current in subsequent cycles because of HOPG surface oxidation was relatively slower in $[BMIM][N(Tf)_2]$ as compared to $[BMIM][HSO_4]$. EC-AFM results also suggest that in the case of $[BMIM][N(Tf)_2]$, intercalation of $[^{-}N(Tf)_2]$ ions occurs only at potentials where HOPG surface oxidation occurs. At potentials lower than the surface oxidation potential, it is difficult for the bulky $[^{-}N(Tf)_2]$ ion to intercalate into the HOPG layers. Because of the smaller size of the $[HSO_4^{-}]$ ion, it can easily intercalate into the interlayer spacing of the HOPG (3.35 Å) and lead to reversible intercalation−deintercalation with change in the electrochemical potential. To see the degradation products, after the three potential hold cycles, the HOPG surface with the IL was left overnight for the degradation products to settle. After removal of the IL from the HOPG surface from the previous day, the surface was washed with ethanol before AFM imaging. Figure 9 shows the AFM image of the HOPG surface. Carbon nanoparticles 30−80 nm in size (as shown by the size distribution analysis in the inset in Figure 9) can be seen adsorbed on the HOPG surface. The adsorbed particles are larger in size but are lesser in density compared to that in the case of $[BMIM][HSO_4]$ IL (Figure 5). This observation further supports our prediction that the carbon oxidation process is slower in $[BMIM][N(Tf)_2]$. Figure 10 shows the photographs of the two ILs before and after the potential hold cycles. It can be seen that the original colorless $[BMIM][HSO_4]$ IL has become brown in color whereas colorless $[BMIM][N(Tf)_2]$ IL remained colorless after the potential hold cycles. This could

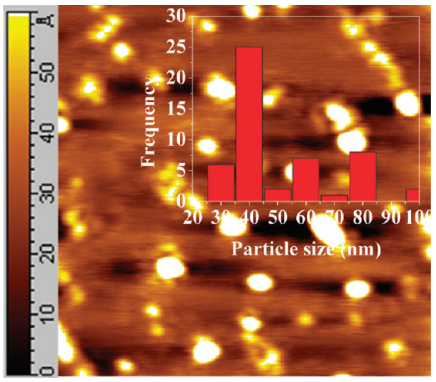

Figure 9. AFM image of the carbon nanoparticles on the HOPG surface. The AFM image was recorded after three potential hold cycles in pure $[BMIM][N(Tf)_2]$ and by allowing the carbon nanoparticles to settle on the HOPG surface overnight. The HOPG surface was washed with ethanol and was dried before AFM imaging. Scan area and height scale for the image are $1 \times 1\ \mu m^2$ and 60 Å, respectively.

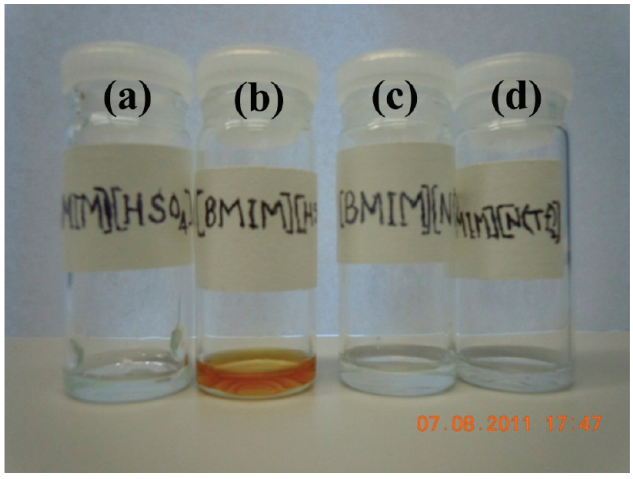

Figure 10. Photograph of the sample vial containing $[BMIM][HSO_4]$ (a) before and (b) after three potential hold cycles and $[BMIM][N(Tf)_2]$ (c) before and (d) after three potential hold cycles.

be due to the greater intercalation of $[HSO_4^{-}]$ ions into the HOPG layers and to a higher degradation rate of HOPG steps in $[BMIM][HSO_4]$ IL observed before. Similar observations were made during the formation of IL-functionalized carbon nanomaterials by ionic liquid-assisted electrochemical exfoliation of graphite in 1-butyl-3-methyl imidazolium tetrafluoroborate $[BMIM][BF_4]$ IL by Lu et al.[35] where colorless $[BMIM][BF_4]$ changed to brown after the electrochemical exfoliation process. However, in their experiments, IL/water mixtures were used as electrolytes to perform electrochemical exfoliation of graphite. In pure $[BMIM][BF_4]$, high activation voltages of 6−8 V were required to initiate the exfoliation of graphite forming a bucky gel from which carbon nanoparticles and graphene sheets were isolated. They proposed oxidation to primarily occur at graphite edge sites, grain boundaries, or defect sites resulting in an opening up of the edge sheets thereby facilitating intercalation of BF_4 ions into graphite causing the depolarization and expansion of the graphite anode. Figure 11 summarizes the processes occurring at the HOPG surface at various potentials in the two ILs used.

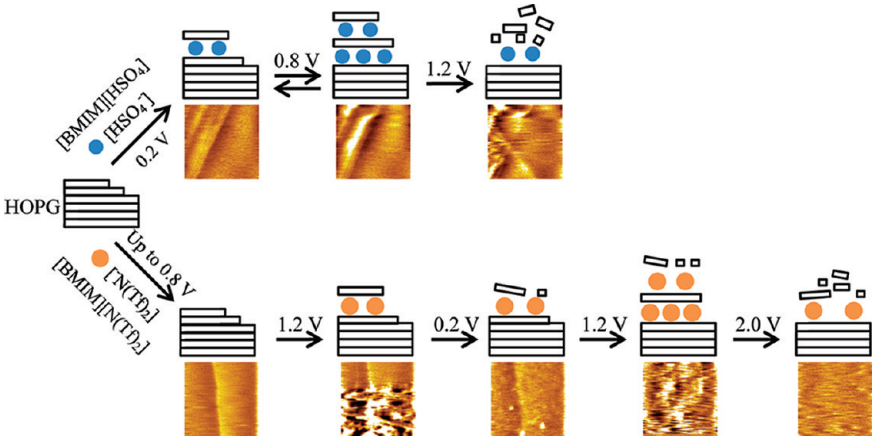

Figure 11. Summary of the EC-AFM investigation of electrochemical intercalation−deintercalation of the anions into HOPG in pure [BMIM][HSO_4] and [BMIM][$N(Tf)_2$] ILs.

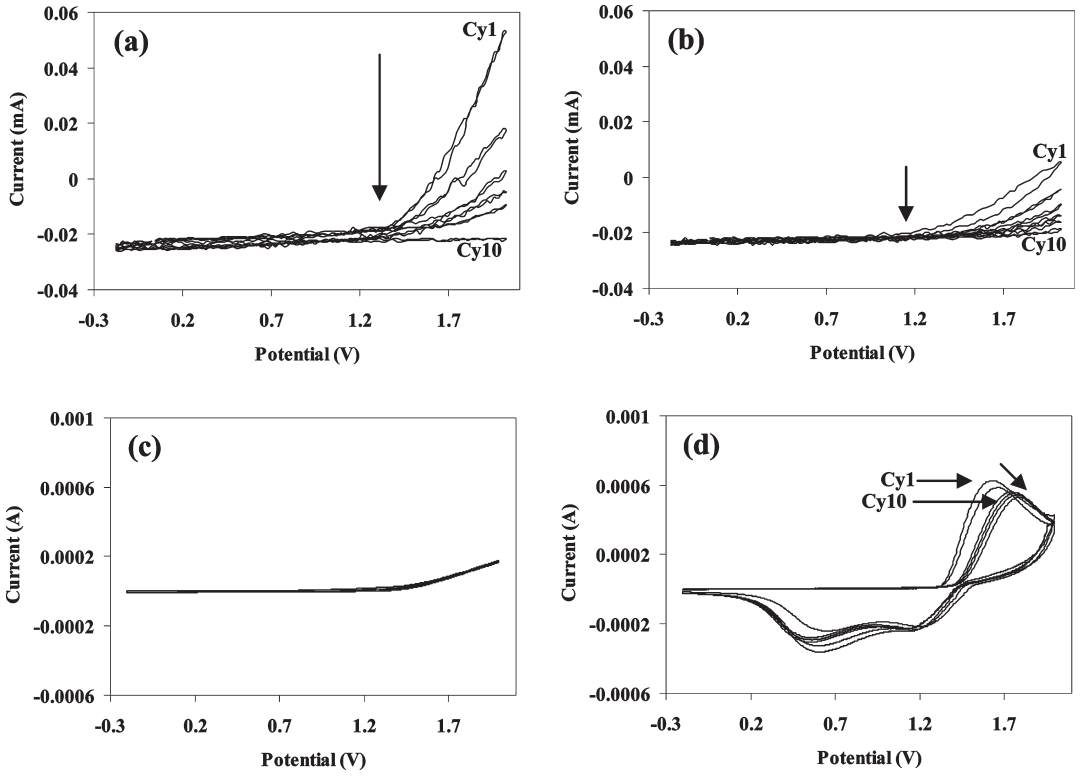

Figure 12. Cyclic voltammograms (CVs) of HOPG for the various potential cycles in pure (a) [BMIM][HSO_4] and (b) [BMIM][$N(Tf)_2$] ILs in the electrode configuration shown in Scheme 2a where only a few HOPG steps are exposed and in pure (c) [BMIM][HSO_4] and (d) [BMIM][$N(Tf)_2$] ILs in the electrode configuration shown in Scheme 2b where many HOPG steps are exposed.

Cyclic Voltammetry. To understand the mechanism of intercalation−deintercalation of ions into HOPG layers in pure [BMIM][HSO_4] and [BMIM][$N(Tf)_2$] ILs, cyclic voltammograms (CVs) of HOPG in the same configuration as used during the EC-AFM studies were recorded. During the EC-AFM studies, a freshly cleaved HOPG surface having fewer steps as shown in Scheme 2a was used. As shown by the EC-AFM images in the previous sections, at 1.2 V, these steps are oxidized leading to its degradation in both the ILs used. On repetition of these oxidation cycles, most of the steps are oxidized leaving behind only basal planes on the HOPG surface. Figure 12a and b shows the CVs of HOPG in pure [BMIM][HSO_4] and [BMIM][$N(Tf)_2$] ILs. CVs show a strong anodic peak around 1.2 V because of surface oxidation of HOPG in both the ILs. This result supports EC-AFM results where drastic changes of the HOPG surface morphology were observed at 1.2 V. As the step edges on the HOPG surface have higher activity, these are prone to oxidation at this potential. From the CVs, it is interesting to note that the anodic current due to HOPG step oxidation decreases in subsequent oxidation cycles for both the ILs. These results support our earlier prediction that the anodic current at 1.2 V is due to HOPG step oxidation, and with subsequent oxidation cycles, these steps are degraded. The

dx.doi.org/10.1021/jp203833v |J. Phys. Chem. C 2011, 115, 17429–17439

Scheme 2. Experimental Configuration Used during the (a) EC-AFM Measurements and Cyclic Volammetric (CV) Measurement in Figure *12*a, b and (b) during the CV Measurement in Figure *12*c, d

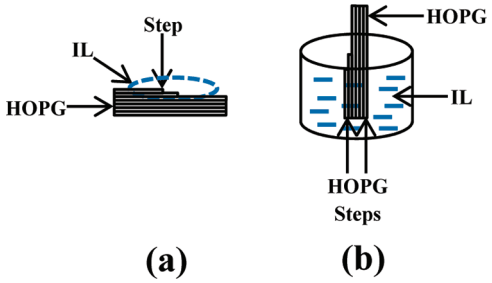

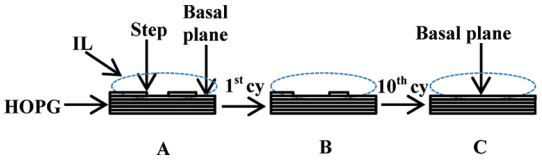

Figure 13. Model showing the steps involved during the degradation of step edges on HOPG during the electrochemical intercalation−deintercalation process in pure ILs. (A) The initial condition, (B) after the first oxidative cycle where we can see little degradation of the step, and (C) after 10 cycles where most of the steps on HOPG surface are degraded and only basal planes remain.

CVs for HOPG in both the ILs show that after 10 cycles, the CVs became almost flat in [BMIM][HSO_4], whereas in [BMIM]-[$N(Tf)_2$], there is still a small anodic peak visible. These results suggest that most of the steps on the HOPG surface are oxidized in both the ILs, and only basal planes, which are less prone to oxidation, remain on the HOPG surface. This is shown by the model in Figure 13. Another interesting point from the CVs is that the decrease in the anodic current because of step edge oxidation of HOPG is slower in pure [BMIM][$N(Tf)_2$] as compared to [BMIM][HSO_4]. The decrease in the anodic current on going from the 1st cycle to the 10th cycle in [BMIM][HSO_4] is 140%, whereas it is 2.4% in [BMIM][$N(Tf)_2$]. The possible reason for this could be due to the nature of these ILs. [BMIM][HSO_4] is a hydrophilic IL. Step edges on the HOPG surface are fairly hydrophilic in nature,[36] and hence in [BMIM][HSO_4], step edges on the HOPG surface are in a favorable environment for electrochemical surface oxidation as compared to [BMIM][$N(Tf)_2$] which is a hydrophobic ionic liquid. This is why it was possible to sequentially remove carbon layers from the HOPG surface in pure [BMIM][$N(Tf)_2$] during the EC-AFM observations in Figure 8 as the HOPG surface oxidation process was slower as compared to that in [BMIM][HSO_4] where mostly degradation of the HOPG surface was observed because of oxidation of multiple carbon layers (Figure 4). To further support our mechanism, CVs of HOPG in the two ILs were also recorded in a different configuration as shown in Scheme 2b where many HOPG layers were exposed. This way, there are many HOPG layers for intercalation of ions in ILs and subsequent HOPG step edge oxidation. Figure 12c and d shows the CVs of HOPG recorded in pure [BMIM][HSO_4] and [BMIM][$N(Tf)_2$] ILs, respectively. As seen from Figure 12c and d, there was only a slight decrease in the anodic peak current because of HOPG step edge oxidation in [BMIM][HSO_4] and [BMIM]-[$N(Tf)_2$] for subsequent cycles as there are many step edges of HOPG exposed in this configuration. This supports our mechanism discussed earlier. Another interesting point is that the shape of the voltammogram in Figure 12d is significantly different from that in Figure 12b. Here, a broader peak during the anodic cycle and two distinct peaks during the cathodic cycle are observed. This suggests that in this configuration possibly there is intercalation of [$-N(Tf)_2$] anion into the HOPG layers as there are many layers exposed and also there could be defects at the edges which may have led to larger interlayer spacing between the HOPG layers facilitating the intercalation. During molecular dynamics simulation studies of microscopic structures of room-temperature ionic liquid [BMIM][PF_6] on hydrophobic graphite surface, Sha et al.[37] found that the imidazolium ring and the butyl tail of the cation [$BMIM^+$] of the IL bottom layer lie flat on the graphite surface because of strong interaction between the cation and the graphite surface. Because of the very good intercalation property of [HSO_4^-] ions into graphite, there is electrochemical potential induced intercalation−deintercalation of [HSO_4^-] ions into graphite without any significant chemical interaction with graphite and hence no change in the CV of HOPG in [BMIM][HSO_4] IL. However, in the case of [$-N(Tf)_2$] anions, there is probably adsorption of these ions onto the graphite surface mostly on the HOPG steps because of strong electrostatic interaction between the positively charged C atoms on graphite and the negatively charged N in [$-N(Tf)_2$] anion, and the redox peaks observed in the CV of HOPG in [BMIM][$N(Tf)_2$] IL are probably due to the redox chemistry of adsorbed [$-N(Tf)_2$] anion onto the graphite surface.

CONCLUSIONS

Using EC-AFM, reversible morphological changes during electrochemical intercalation−deintercalation of [HSO_4^-] ions into HOPG could be monitored in pure [BMIM][HSO_4] IL up to +0.8 V. It was possible to get the quantitative estimate of the amount of thickness changes on the HOPG surface during the intercalation−deintercalation process. No intercalation into HOPG and hence no morphological changes were observed in pure [BMIM][$N(Tf)_2$] IL up to +0.8 V. Above 0.8 V, degradation of the steps on the HOPG surface to form carbon nanoparticles was observed in both the ILs used. In [BMIM][HSO_4], HOPG step edge degradation was faster, whereas in [BMIM]-[$N(Tf)_2$], it was possible to remove carbon layers sequentially during the oxidative potential cycles. This process could find potential applications in catalysis and electroanalysis where it is possible to prepare active carbon electrodes in situ.

AUTHOR INFORMATION

Corresponding Author

*E-mail: zeng@oakland.edu. Tel: 248-370-2881. Fax: 248-370-2321.

ACKNOWLEDGMENT

X. Zeng likes to thank Dr. Gary Baker for help regarding ionic liquid synthesis and the grant support from NIOSH (R21009099) and ONR (N000141010734) for this work.

REFERENCES

(1) Alsmeyer, D. C.; McCreery, R. L. *Anal. Chem.* **1992**, *64*, 1528–1533.

(2) Goss, C. A.; Brumfield, J. C.; Irene, E. A.; Murray, R. W. *Anal. Chem.* **1993**, *65*, 1378–1389.

(3) Hathcock, K. W.; Brumfield, J. C.; Goss, C. A.; Irene, E. A.; Murray, R. W. *Anal. Chem.* **1995**, *67*, 2201–2206.
(4) Alliata, D.; Kotz, R.; Haas, O.; Siegenthaler, H. *Langmuir* **1999**, *15*, 8483–8489.
(5) Sheldon, R. *Chem. Commun.* **2001**, 2399–2407.
(6) Armand, M.; Endres, F.; MacFarlane, D. R.; Ohno, H.; Scrosati, B. *Nat. Mater.* **2009**, *8*, 621–629.
(7) MacFarlane, D. R.; Pringle, J. M.; Howlett, P. C.; Forsyth, M. *Phys. Chem. Chem. Phys.* **2010**, *12*, 1659–1669.
(8) Endres, F.; Hofft, O.; Borisenko, N.; Gasparotto, L. H.; Prowald, A.; Al-Salman, R.; Carstens, T.; Atkin, R.; Bund, A.; Abedin, S. Z. E. *Phys. Chem. Chem. Phys.* **2010**, *12*, 1724–1732.
(9) Bhushan, B.; Palacio, M.; Kinzig, B. *J. Colloid Interface Sci.* **2008**, *317*, 275–287.
(10) Bovio, S.; Podesta, A.; Lenardi, C.; Milani, P. *J. Phys. Chem. B* **2009**, *113*, 6600–6603.
(11) Su, Y.-Z.; Fu, Y.-C.; Yan, J.-W.; Chen, Z.-B.; Mao, B.-W. *Angew. Chem., Int. Ed.* **2009**, *48*, 5148–5151.
(12) Atkin, R.; El Abedin, S. Z.; Hayes, R.; Gasparotto, L. H. S.; Borisenko, N.; Endres, F. *J. Phys. Chem. C* **2009**, *113*, 13266–13272.
(13) Atkin, R.; Warr, G. G. *J. Phys. Chem. C* **2007**, *111*, 5162–5168.
(14) Liu, Y.; Zhang, Y.; Wu, G.; Hu, J. *J. Am. Chem. Soc.* **2006**, *128*, 7456–7457.
(15) Sung, J.; Jeon, Y.; Kim, D.; Iwahashi, T.; Seki, K.; Iimori, T.; Ouchi, Y. *Colloids Surf., A* **2006**, *284*, 84–88.
(16) Baldelli, S. *J. Phys. Chem. B* **2003**, *107*, 6148–6152.
(17) Fitchett, B. D.; Conboy, J. C. *J. Phys. Chem. B* **2004**, *108*, 20255–20262.
(18) Ozawa, R.; Hayashi, S.; Saha, S.; Kobayashi, A.; Hamaguchi, H. *Chem. Lett.* **2003**, *32*, 948–949.
(19) Hayashi, S.; Ozawa, R.; Hamaguchi, H. *Chem. Lett.* **2003**, *32*, 498–499.
(20) Bowers, J.; Vergara-Gutierrez, M. C.; Webster, J. R. P. *Langmuir* **2004**, *20*, 309–312.
(21) Zhang, F.-C.; Sha, M.-L.; Ren, X.-P.; Wu, G.-Z.; Hu, J.; Zhang, Y. *Chin. Phys. Lett.* **2010**, *27* (8), 86101–86104.
(22) Yokota, Y.; Harada, T.; Fukui, K. *Chem. Commun.* **2010**, *46*, 8627–8629.
(23) Endres, F.; Freyland, W. *J. Phys. Chem. B* **1998**, *102*, 10229–10233.
(24) Carlin, R. T.; Fuller, J.; Kuhn, W. K.; Lysaght, M. J.; Trulove, P. C. *J. Appl. Electrochem.* **1996**, *26*, 1147–1160.
(25) Gupta, N.; Sonu; Kad, G. L.; Singh, J. *Catal. Commun.* **2007**, *8*, 1323–1328.
(26) Zhang, Q. B.; Hua, Y. X. *Electrochim. Acta* **2009**, *54*, 1881–1887.
(27) Holbrey, J. D.; Reichert, W. M.; Rogers, R. D. *Dalton Trans.* **2004**, 2267–2271.
(28) Burrell, A. K.; Del Sesto, R. E.; Baker, S. N.; McCleskey, T. M.; Baker, G. A. *Green Chem.* **2007**, *9*, 449–454.
(29) Baker, S. N.; McCleskey, T. M.; Pandey, S.; Baker, G. A. *Chem. Commun.* **2004**, 940–941.
(30) Jin, H.; O'Hare, B.; Dong, J.; Arzhantsev, S.; Baker, G. A.; Wishart, J. F.; Benesi, A. J.; Maroncelli, M. *J. Phys. Chem. B* **2008**, *112* (1), 81–92.
(31) Hahn, M.; Barbieri, O.; Campana, F. P.; Kotz, R.; Gallay, R. *Appl. Phys. A: Mater. Sci. Process.* **2006**, *82*, 633–638.
(32) Ka, B. H.; Oh, S. M. *J. Electrochem. Soc.* **2008**, *155*, A685–A692.
(33) Aronson, S.; Lemont, S.; Weiner, J. *Inorg. Chem.* **1971**, *10* 1296–1298.
(34) Campana, F. P.; Buqa, H.; Novak, P.; Kotz, R.; Siegenthaler, H. *Electrochem. Commun.* **2008**, *10*, 1590–1593.
(35) Lu, J.; Yang, J.-X.; Wang, J.; Lim, A.; Wang, S.; Loh, K. P. *ACS Nano* **2009**, *3*, 2367–2375.
(36) Losic, D.; Martin, L. L.; Anguilar, M-I; Small, D. H. *Biopolymers* **2006**, *84*, 519–526.
(37) Sha., M.; Zhang, F.; Wu, G.; Fang, H.; Wang, C.; Chen, S.; Zhang, Y.; Hu, J. *J. Chem. Phys.* **2008**, *128*, 134504.